

Irreversible shape distortions by flux-pinning-induced magnetostriction in hard type-II superconductors

T.H. Johansen, J. Lothe and H. Bratsberg

Department of Physics, University of Oslo, P.O. Box 1048, Blindern, 0316 Oslo 3, Norway.

(November 12, 2017)

Exact analytical results are obtained for the flux-pinning-induced magnetostriction in long cylinders of type-II superconductors placed in a parallel magnetic field. New effects are found regarding the irreversible deformation of the cross-sectional area: Whereas the magnetostriction of a circular cylinder is shape conserving, it is shown that a square cross-section deforms with considerable distortion. During a field cycle both concave, convex, and even more complicated distortions are predicted. The strong implications for the interpretation of dilatometric observations are pointed out. The main results obtained for both the circular and square geometry are valid for any critical-state model, $j_c = j_c(B)$, and we use the Bean model for illustration and discussion.

PACS numbers: 74.25.Ha, 74.60.Ge, 74.60.Jg

It was discovered by Ikuda and coworkers¹ that high temperature superconductors (HTSCs), when placed in a magnetic field, can respond by a giant magnetostriction. Relative changes in sample size as large as 10^{-4} were observed in single crystals of $\text{Bi}_2\text{Sr}_2\text{CaCu}_2\text{O}_8$. To explain this deformation, which is about two orders of magnitude larger than values reported for conventional superconductors,² they considered the stress exerted on the crystal by pinned vortices. Treating the crystal as an infinite slab of half-width, w , placed in a parallel applied field, B_a/μ_0 , the pinning-induced magnetostriction in the transverse direction was derived from the critical-state model to be

$$\Delta w/w = (2c\mu_0 w)^{-1} \int_0^w [B^2(x) - B_a^2] dx, \quad (1)$$

where c is the elastic constant and $B(x)$ the local induction. As evident from eq.(1), and also pointed out immediately by Ikuta et al., the pinning-induced magnetostriction is intimately related to the magnetization, and consequently should display similar irreversible characteristics. Following the discovery, the giant magnetostriction was observed also in single crystals of other HTSC materials,³ thus establishing the effect as being a general phenomenon which, like the magnetization, can provide important information about the pinning properties.

Magnetostriction, as dilatations in general, are most frequently measured by displacive sensors like e.g. a capacitance dilatometer cell. Such sensors provide an electrical signal which normally represents the variation in the end-to-end dimensions of a sample.⁴ Although very high sensitivities (10^{-12} m) can be achieved, the cells are usually designed so that distortions in shape are not accounted for, or they may even influence the measurements in an uncontrolled way. Up to now, shape distortions in connection with the pinning-induced magnetostriction were never considered, and all data analysis

has been based on the relation eq.(1) valid for plane strain deformations only.

In this letter we show that the pinning-induced stress indeed leads to significant shape distortions even in the simple geometry of an infinitely long isotropic cylinder with square cross-section. For comparison we also present the exact solution of the magneto-elastic problem for the circular cylinder where shape is conserved.

From electrodynamics the force which drives the vortices into the material is given by $\mathbf{j} \times \mathbf{B}$ per unit volume. For HTSCs in the mixed state under practical conditions the current density, \mathbf{j} , is usually set equal to $(\nabla \times \mathbf{B})/\mu_0$ as the thermodynamic field can be well approximated by \mathbf{B}/μ_0 .⁵ In the critical-state model one has $|\mathbf{j}| = j_c$, and a non-uniform distribution of pinned flux transmits onto the crystal a volume force density equal to $\mathbf{f} = \mathbf{j}_c \times \mathbf{B}$. In the two geometries under consideration the symmetry of the force field is quite different, see Fig.1. In contrast to the simple radial distribution shown in (a), the square cylinder in (b) is divided into four regions each containing distributed forces pointing the same direction. Moreover, in both cases the cylinder generally has additional divisions into shells where the forces alternate in sign - or they can even vanish - all depending on the magnetic prehistory. In all such states the force exerted on the material per unit volume is given by

$$\mathbf{f} = (\nabla \times \mathbf{B}) \times \mathbf{B}/\mu_0 = -(2\mu_0)^{-1} \nabla B^2. \quad (2)$$

The last form, expressing a purely magnetic free energy of the vortex lattice, is used in the present calculations. In the analysis the strains are assumed well below the fracture limit allowing linear elasticity theory, and hence the principle of superposition, to be applicable.

In the circular cylinder the rotational symmetry implies that the deformation is described by a radial displacement field, $u_r(r)$. The non-vanishing components of the strain are $e_r = u_r'(r)$ and $e_\theta = u_r/r$, which are related

to the stress components, σ_θ and σ_r by $Ee_r = \sigma_r - \nu\sigma_\theta$ and $Ee_\theta = \sigma_\theta - \nu\sigma_r$. Here E and ν is the Young's modulus and Poisson's ratio, respectively.

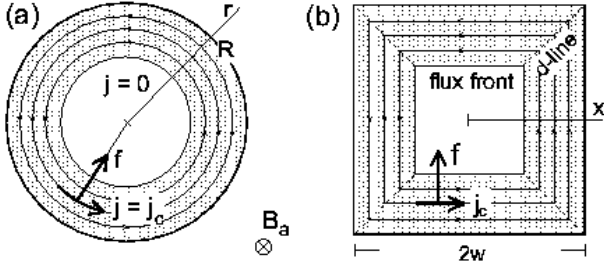


FIG. 1. Flux penetration and current flow pattern in a circular (a) and square (b) cylinder in the critical-state model. The indicated magnetized states contain a flux front, illustrating that the cylinders generally are divided in shells with different volume forces.

The condition of static equilibrium is that $(d\sigma_r/dr) + (\sigma_r - \sigma_\theta)/r + f = 0$, which in terms of the displacement field is expressed as

$$u_r'' + \frac{1}{r} u_r' - \frac{1}{r^2} u_r + \frac{1-\nu^2}{E} f(r) = 0. \quad (3)$$

Integration twice, and using that $u_r(0) = 0$, gives

$$u_r(r) = -\frac{1-\nu^2}{E} \frac{1}{r} \int_0^r r' F(r') dr' + Cr, \quad (4)$$

where $F(r) \equiv \int_0^r f(r') dr' = [B^2(0) - B^2(r)]/2\mu_0$. With the constant C determined by the free surface condition $\sigma_r(r = R) = 0$, the result becomes

$$u_r(r) = -\frac{1-\nu^2}{2E\mu_0} \left\{ \left[B_a^2 - \frac{1-\nu}{R^2} \int_0^R r' B^2(r') dr' \right] r - \frac{1+\nu}{r} \int_0^r r' B^2(r') dr' \right\}, \quad (5)$$

which is the exact solution from which a complete stress-strain picture can be expressed in terms of the flux density $B(r)$. E.g., the radial stress is given by

$$\sigma_r(r) = \frac{1}{2\mu_0} \left\{ B^2(r) - B_a^2 + \frac{1-\nu}{R^2} \left[\int_0^R r' B^2(r') dr' - \frac{R^2}{r^2} \int_0^r r' B^2(r') dr' \right] \right\}. \quad (6)$$

The eqs.(5) and (6) generalizes expressions for u_r and σ_r derived recently⁶ only for the Bean model, $j_c(B) = \text{constant}$. We emphasize that our results are valid for any critical-state model.

For the external dilatation, $\Delta R/R = u_r(R)/R$, one obtains from eq.(5)

$$\frac{\Delta R}{R} = \frac{1-\nu}{E\mu_0 R^2} \int_0^R r [B^2(r) - B_a^2] dr. \quad (7)$$

This formula for the pinning-induced magnetostriction of a circular cylinder, first found by Johansen et al.,⁷ is very similar to the expression in eq.(1) for the slab. The extra factor r in the integral is a simple modification, which one finds analogously in the expressions for the critical-state magnetization. The factor $1-\nu$ reflects the stronger constraint on free expansion for the cylinder as compared to the slab.

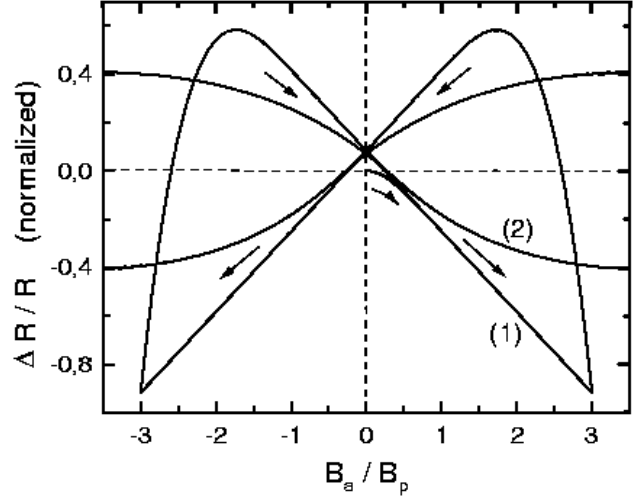


FIG. 2. Magnetostriction, $\Delta R/R \times (1-\nu)(\mu_0 j_0 R)^2/E\mu_0$, as function of applied field for a circular cylinder with $j_c = j_0 \exp(-|B|/B_0)$. Curve (1); $B_0 = \infty$ i.e. the Bean model and (2); $B_0 = \mu_0 j_0 R/0.3$. The field axis is normalized by the full penetration field $B_p = B_0 \ln(1 + \mu_0 j_0 R/B_0)$.

From eq.(7) analytical expressions for the various branches of magnetostriction hysteresis loops are readily derived. Figure 2 shows how $\Delta R/R$ depends on the applied field for two commonly used critical-state models. As B_a runs through a complete cycle $\Delta R/R$ displays a huge hysteresis loop where in the Bean model case both the main ascending and descending branches are linear and provided a sufficiently high maximum field. Among other features of the Bean model results is that the maximum remanent magnetostriction is given by

$$(\Delta R/R)_{\text{rem}} = (1-\nu)(12E)^{-1} \mu_0 j_c^2 R^2. \quad (8)$$

Since the remanent state has no contribution from reversible components, the above relation provides a means to infer j_c from magnetostriction measurements. In the field range where the main branches are linear the vertical width of the hysteresis loop equals

$$(\Delta R/R)_\downarrow - (\Delta R/R)_\uparrow = 2(1-\nu)(3E)^{-1} R j_c B_a. \quad (9)$$

Note in particular that if the hysteresis width is normalized by $(\Delta R/R)_{\text{rem}}$ the value of j_c can be found from the

slope in a plot versus B_a without knowledge of the elastic constants. The normalized width is simply $8B_a/\mu_0 j_c R$, a result analogous to the extensively used Bean model relation between j_c and the width of the magnetization loop. Conversely will measurements of magnetostriction allow determination of the elastic parameter $(1-\nu)/E$ if j_c is known from other measurements.

The more curved hysteresis loop resulting from the exponential model, $j_c = j_0 \exp[-|B|/B_0]$, graph (2) in Fig.2, is usually a better description of observed magnetostrictive behavior in HTSCs.^{3,8} An extensive analysis with various $j_c(B)$ -functions is subject of a forthcoming paper, where also the rather lengthy expressions for the different branches in Fig.2, is presented.

A final remark on the circular case is that the integral in eq.(7) also can be written as $\int_0^R r^2 f(r) dr$, i.e., the $\Delta R/R$ is given as the second moment of the volume force distribution just as the j_c -loops determine the magnetization. One could be tempted to generalize the relation to other cylindrical geometries, and thus allow for a simple unified treatment as done in magnetization calculations.⁹ However, such generalization would be incorrect, as will become evident as we now turn to the square cross-section case.

A different approach is chosen to analyze the magneto-elastic problem of the square cylinder. Within the linear elasticity approximation one can separate the treatment into an infinite number of deformations produced by infinitesimal square loops of the force field (Fig.1 b). The final result is obtained by superimposing the elastic response of the whole cylinder to each force loop. For this to be a useful approach one needs a way of adding these deformations in a coherent manner. We first show that this indeed is feasible for the square cylinder.

Consider the effect of a square force loop of width dx with sides a distance x from the origin (Fig.3). The material enclosed by the loop will experience only a normal stress, and the deformation becomes a plane strain. The elastic response of the enclosed area is given by $Ee_1 = \sigma_1 - \nu\sigma_2$ and $Ee_2 = \sigma_2 - \nu\sigma_1$, where e_1 , e_2 and σ_1 , σ_2 are the plane strain and normal stress components, respectively. It immediately follows that the relative change in the square area equals $e_1 + e_2 = -(1-\nu)E^{-1} 2p$ where $p = -(\sigma_1 + \sigma_2)/2$ is the two-dimensional pressure. The enclosed area deforms under this pressure into another square so that a constant gap δg is created along the loop. Using that $p = f(x)dx$, the size of this virtual gap becomes

$$\delta g = (1-\nu)E^{-1} x f(x) dx . \quad (10)$$

The sign of δg is so that a positive value represents a void space, whereas a negative δg corresponds to an expansion of the inner square.

The contribution from this elementary deformation to the strain of the whole body is obtained by recombining

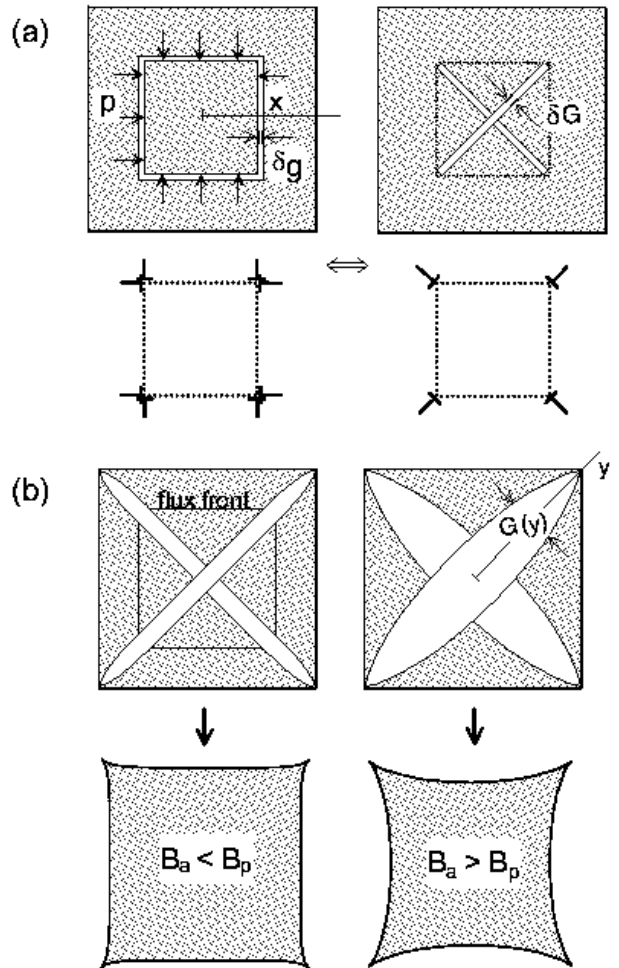


FIG. 3. (a) Partial effect of the volume force in a square cylinder. By the shown transformation the elastic problem can be treated analytically using superposition, see text. (b) Schematic picture of the deformation (strongly amplified) of a square cylinder in the case of (left) incomplete and (right) complete flux penetration.

(“gluing together”) the parts on each side of the virtual gap. The resulting strained state is equivalent to having a pair of edge dislocations in each corner of the loop. As each pair can be replaced by one dislocation directed along the diagonal, we conclude that the original gap space can be replaced by two slits of width $\delta G = \delta g \sqrt{2}$ forming a central cross. By this transformation the integral effect of the entire force field can be determined analytically as follows. Let y denote the distance from the center to a point on a diagonal. At this point the total gap, G , is an accumulation of the gaps δG created from y and out to the corner $y = w\sqrt{2}$. The total result is therefore given by

$$\frac{G(y)}{w\sqrt{2}} = \sqrt{2} \frac{1-\nu}{E\mu_0} \int_{y/\sqrt{2}}^w B(x)B'(x)x dx . \quad (11)$$

The full deformation is now obtained by "gluing" the virtually disrupted material together. Since $G'(y) \propto B j_c y$ it follows that $G(y)$ is not a linear function, thus proving that the pinning-induced magnetostriction does not conserve shape in the square case.

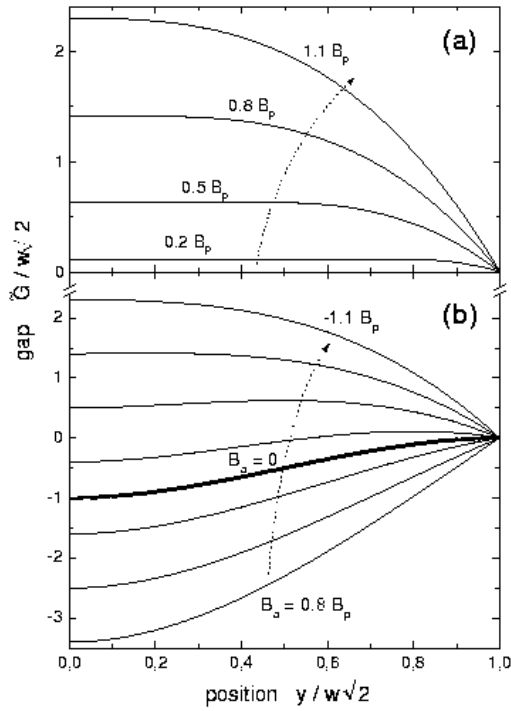


FIG. 4. Gap shape at various stages of flux penetration. (a) Increasing field (B_a indicated) and (b) decreasing field for $B_a/B_p = 0.8, 0.5, 0.2, 0$ (thick line), $-0.2, -0.5, -0.8 -1.1$.

The eq.(11) allows the gap to be calculated. In the Bean model along the increasing field branch one finds for $\tilde{G} \equiv G E \mu_0 (1 - \nu)^{-1} B_p^{-2}$ the expression

$$\frac{\tilde{G}(y)}{w\sqrt{2}} = 3\left[1 - \left(\frac{y}{w\sqrt{2}}\right)^2\right] \left(\frac{B_a}{B_p} - 1\right) + 2 - 2\left(\frac{y}{w\sqrt{2}}\right)^3, \quad (12)$$

in the penetrated region. In the central Meissner area the gap is constant. The behavior is shown in Fig.4 a, and representative examples of the resulting concave deformations are illustrated qualitatively in Fig.3 b. For the fully penetrated state one sees from eq.(12) that $G(y)$ grows linearly with B_a , while at the same time $G = 0$ at the corners. This produces a deformation where the concave character grows steadily with the applied field.

The behavior of $\tilde{G}(y)$ for descending applied field is shown in Fig.4 b. The deformation along this branch is evidently more diverse even when we omit the stage following immediately after field reversal. The shown graphs represent only stages where j_c is reversed throughout the sample. The profiles with negative \tilde{G} gives rise to convex deformations. The convexity persists all the way down to the remanent state, where the distortion near the corners is vanished. Then, as the field is reversed there is an interval where the behavior is governed by a

$G(y)$ with an oscillatory shape, thus giving a mixed type of deformation. As the reverse field increases in magnitude the shape again becomes concave. For $B_a \leq -B_p$ the sample shape follows the same development as during the field increase.

In conclusion, we have investigated and compared the pinning-induced magnetostriction in two important geometries. In contrast to the shape-conserving circular case, which could be solved exactly, the existence of current discontinuity(d)-lines in the square case complicates the behavior by producing shape distortion. We have predicted the appearance of convex, concave and even more complicated types of deformations where the distortion is of the same order of magnitude as the overall striction. Since in most cases HTSC crystals have a rectangular shape, which always lead to d-lines in the critical-state, the distortion could easily lead to misinterpretation of dilatometric measurements. The problem should be minimized by (i) having a high aspect ratio rectangular shape so that the central part of the sample is described approximately by a plane strain deformation, and (ii) designing the displacive sensor with a local contact to the long side of the rectangle in order to avoid distorted corner regions. Full analysis of the proper corrections will clearly require numerical work.

The authors acknowledge discussions with Yu. Galperin, and financial support from The Research Council of Norway.

- ¹ H. Ikuta, N. Hirota, Y. Nakayama, K. Kishio and K. Kitazawa, Phys. Rev. Lett. **70**, 2166 (1993).
- ² G. Brändli and R. Griessen, Phys. Rev. Lett. **22**, 534 (1969); G. Brändli, Phys. Kond. Mater. **11**, 93 (1970).
- ³ N. Hirota et al., J. Superconductivity **7** 283, (1994). A. Schmidt et al., Physica B **194-196**, 1787 (1994); A. Nabilalek et al., Supercond. Sci. Technol. **10** 786 (1997)
- ⁴ R. Jones and J. Richards, J. Phys. E **6**, 589 (1973); G. Brändli and R. Griessen, Cryogenics **13**, 299 (1973); T.H. Johansen, J. Feder and T. Jössang, Rev. Sci. Instr. **57**, 1168 (1986).
- ⁵ E. Zeldov, J.R. Clem, M. McElfresh and M. Darwin, Phys. Rev. B **49** 9802 (1994)
- ⁶ Y. Ren, R. Weinstein, J. Liu., R.P. Sawh and C. Foster Physica C, **251** 15 (1995).
- ⁷ T.H. Johansen, J. Lothe and H. Bratsberg, in "Fourth Euro Ceramics - High T_c Superconductors, Part II", eds. A Barone, D. Fiorani and A. Tampieri (Faenza, Italy 1995).
- ⁸ H. Ikuta, K. Kishio and K. Kitazawa, J. Appl. Phys. **76**, 4776 (1994).
- ⁹ D.-X. Chen and R.B. Goldfarb, J. Appl. Phys. **66** 2489 (1989); T.H. Johansen and H. Bratsberg, J. Appl. Phys. **77**, 3945 (1994).